Large-proximity-induced anomalous Hall effect in math xmlns="http://www.w3.org/1998/Math/MathML">mrow>msub>mi>Bi/mi>mrow>mn>2/mn>mo>−/mo>mi>x/mi>/mrow>/msub>msub>mi>Sb/mi>mi>x/mi>/msub>msub>mi>Te/mi>mrow>mn>3/mn>mo>−/mo>mi>y/mi>/mrow>/msub>msub>mi>Se/mi>mi>y/mi>/msub>mo>//mo>msub>mi>Cr/mi>mn>2/mn>/msub>msub>mi>Ge/mi>mn>2/mn>/msub>msub>mi>Te/mi>mn>6/mn>/msub>/mrow>/math> heterostructure prepared by film transfer method

Kazumasa Nagata, Stephane Yu Matsushita, Xing-Chen Pan, Kim-Khuong Huynh, and Katsumi Tanigaki

Phys. Rev. Materials **5**, 024208 — Published 26 February 2021

DOI: 10.1103/PhysRevMaterials.5.024208

Large-Proximity-Induced Anomalous Hall Effect in $Bi_{2-x}Sb_xTe_{3-y}Se_y/Cr_2Ge_2Te_6$ Heterostructure prepared by Film Transfer Method

Kazumasa Nagata[1], Stephane Yu Matsushita*[,2], Xing-Chen Pan[2], Kim-Khuong Huynh[2],

Katsumi Tanigaki*[2,3]

[1]*Department of Physics, Graduate School of science, Tohoku University, Sendai 980-8578, Japan*

[2]*WPI-Advanced Institute for Materials Research, 2-1-1 Katahira, Aoba-ku, Sendai, Miyagi, 980-8578, Japan*

[3]*Beijing Academy of Quantum Information Sciences, Beijing 100193, China*

KEYWORDS: topological insulator, thin film, anomalous hall effect, proximity effect

ABSTRACT

The magnetic proximity effect is one of the powerful approaches to realize quantum anomalous Hall effect (QAHE) in topological insulators (TIs) targeting at high temperatures. Various TI/ferromagnetic-insulator (FMI) heterostructures have extensively been investigated by using a van der Waals epitaxial growth technique of TI films grown on FMI substrates. However, FMI materials which can be used as a substrate are strictly limited due to the lattice mismatching between TI and FMI, not succeeding to boost the quantization temperature to be higher. Here, we show that, a large anomalous Hall effect (AHE), comparable to the best value so far reported for the heterostructure interfaces fabricated by epitaxial growth techniques, is realized for $Bi_{1.5}Sb_{0.5}Te_{1.7}Se_{1.3}$ (BSTS)/$Cr_2Ge_2Te_6$ (CGT) heterostructure by transferring an epitaxially grown BSTS thin film floating on a ultra-pure water directly on a CGT substrate (wet-transfer method). The fundamental discussions about the nature of magnetic proximity effect were given in the aspect of the quality of the CGT substrate, and the atomic orientation of the TI/CGT interface. The large magnetic proximity effect shown in our present studies can be applicable for a variety of FMI substrates and therefore can pave a route for promoting magnetic-TIs both in basic science and applications.

Main text

1. Introduction

Introducing a ferromagnetic order into topological insulators (TIs) breaks the time-reversal symmetry (TRS) and opens an energy gap on the topological surface Dirac states (TSDSs) [1,2]. One of the intriguing physical phenomena of such magnetic-TIs is the quantized anomalous Hall effect (QAHE) or anomalous Hall effect (AHE), which generate a dissipationless chiral edge electrical transport that holds the promise for revolutionary electronic and spintronic devices [3-8]. The QAHE was first observed by doping magnetic transitional metals, such as Cr or V, into $(Bi_xSb_{1-x})_2Te_3$ (BST) [4]. Afterwards, a lot of studies on magnetic-doped TIs were reported, however, the observation of QAHE has been succeeded only at ultra-low temperatures below 100 mK due to the various disorders created when magnetic dopants are co-doped into TIs [9-11]. As an alternative method, an approach using the magnetic proximity effect is expected to be an effective method to realize QAHE/AHE at a higher temperature [12-25], and is now one of the very attractive cutting-edge research topics.

The concept of the magnetic proximity is to break the TRS of a preserved topological surface via a magnetic coupling at the interface between a ferromagnetic insulator (FMI) and a TI. Being different from the incorporated magnetic elements into TIs, which frequently cause various problems of creation of disordered states in materials, the intrinsic properties of Dirac electrons on the TI surfaces can be expected without structural damage in the case of proximity methodologies. Therefore, QAHE/AHE can be anticipated to be observed at a higher temperature. The proximity-induced AHE has been observed in several FMI/TI hybrid materials so far, such as Bi_2Se_3/EuS [12], $(Bi_xSb_{1-x})_2Te_3/Y_3Fe_5O_{12}$ (BST/YIG) [15,16], and $(Bi_xSb_{1-x})_2Te_3$/CrGeTe$_3$ [20,21,25], BiSbTeSe/GaMnAs [22]. In most of these previous works, a TI thin film was grown on a FMI substrate by molecular beam epitaxy (MBE) method, where the TI film shows a Van der Waals epitaxy growth on FMI substrates (Epi-TI/FMI). While MBE growth technique can provide a well-ordered homogeneous coupling between TI and FMI, the structural and chemical mismatch at the interface between FMI and TI layer inevitably introduces extra defects, preventing the realization of large AHE [20]. Therefore, the choice of a FMI substrate is strictly limited and only the pair of BST and CGT shows a large AHE to date, where the both materials share similar crystal structures ($R\overline{3}$ vs $R\overline{3}m$) with the same anion (Te) [20,21,25]. In order to accelerate the research on the proximity-induced TI/FMI system (large AHE at high temperatures), other fabrication processes having a wider selectability of substrates should be required.

Recently, a new challenge for observing AHE/QAHE has been carried out via the proximity effect using a TI film transferred on a FMI substrate after crystal growth as reported by Che et al. [18]. While the film transfer methods are familiar in fabricating van der Waals heterostructures in 2D materials, such as graphene, no experimental observations of AHE in a TI/FMI system had been reported prior to Che et al.'s work. Such a transfer method of a TI thin film (Trs-TI) could technically be adopted to any substrates, and would be greatly beneficial for both basic science and applications. Although the previous research succeeded in observing AHE in Bi_2Se_3(TI) /YIG(FMI) by transferring a Be_2Se_3 film on a YIG substrate, successful observations of AHE were still in rare cases compared to those in Epi-TI/FMI ones. Several reasons could be considered other than the large carrier number in the BS film, weak magnetization of YIG and/or contaminations at the interface due to the metal ions included in the solvent. Furthermore, the mismatching of the lattice orientation in Trs-TI is larger than that in Epi-TI in general, and how such orientation mismatching at the interface can make an influence on the magnetic proximity is still an important open question. In order to address to these problems and clarify whether the Trs-TI method is relevant to the TI/FMI fabrication, further investigations using a high insulating TI film and a high magnetization FMI realized by better contamination-free transfer technique are required.

Here, we demonstrate that the largest AHE signal for Trs-TI/FMI, comparable to that obtained in the case of Epi-TI/FMI, can be realized by applying the magnetic proximity effect between a high-quality single-crystal film of $Bi_{1.5}Sb_{0.5}Te_{1.7}Se_{1.3}$ (BSTS) and a CGT substrate (Fig. 1a). The non-damaged Trs-BSTS/CGT heterostructure interface is prepared by soaking a single crystal BSTS film epitaxially grown on mica in a ultra-pure water (UPW), being followed by directly transferring the floated BSTS film to CGT substrate, (called a wet-transfer method). Thanks to the high quality interface without any mechanical damages, our Trs-BSTS/CGT exhibits a large anomalous resistivity $R_{AH} = 56.3\ \Omega$ at 7 K, the value of which is around 20 times bigger than that of the previous work on BS/YIG. The anomalous hall angle of our Trs-BSTS/CGT shows a same magnitude to the Epi-BST/CGT ones, indicating that the orientation mismatching of the interface does not make a sizable influence to the magnitude of the proximity effect. The detail discussions about the fundamental nature of the proximity effect was given by the comparison of our results to those in previous work.

2. Experimental

In order to observe a clear anomalous Hall (AH) signal on the surface states, it is important to suppress the contribution from the bulk carriers. In this aspect, BSTS thin film was selected as the host material because it is one of the best bulk insulating TIs and a high-quality thin film can be grown by epitaxial physical vaper-phase deposition (PVD) method, which was reported elsewhere [26, 27]. BSTS single crystal thin films grown on a mica substrate can be easily transferred to other substrates such as Si by dipping them into UPW. with free of damage [26,27]. We applied this wet-transfer technique of BSTS in order to transfer the film onto CGT and fabricate BSTS/CGT heterostructures. Figure 1 shows the preparation processes of the BSTS/CGT heterostructure. First, a single crystal thin film of BSTS with 21 nm in thickness was grown on a mica substrate with a catalyst-free epitaxial PVD method. Then, the BSTS film was exfoliated from the mica substrate by dipping into UPW (21.9 MΩ cm, Direct-Q$^{@}$ 5UV), and transferred to a CGT substate, which was prepared by a self-flux method of Te. After the film-transfer process, the BSTS/CGT sample was introduced into a vacuum oven and annealed at 150℃ for 1 hour under the pressure of 10^{-1} Pa to dry the sample. All transport measurements were carried out by a Physical Parameters Measurement System (PPMS, Quantum Design).

3. Results and Discussions

A. Raman spectra of BSTS film for each process.

Figure 2 shows the Raman spectra of BSTS film and the CGT corresponding to each preparation process. The pristine CGT showed two strong peaks at 110 cm^{-1} and 135 cm-1 and three weak peaks at 77, 212, 233 and 293 cm^{-1}. Those frequencies are consistent to the previous report on the cleaved CGT [28]. On the other hand, the pristine BSTS film exhibited three peaks at 64, 105, and 152 cm^{-1}, whose frequencies are consistent to our previous works [26,29]. The positions of the peaks of the BSTS film did not change before and after transferring the film on to the CGT substrate and annealing, while additional peaks from CGT substrate were detected for the BSTS/CGT heterostructure. The whole spectra curvature of the BSTS/CGT can be well reproduced by the simple summation of Raman spectra of both pristine BSTS and CGT, as shown in Fig. 2 (b). There results indicates that the crystal structure and the chemical components of the BSTS film do not change during the preparation processes of BSTS/CGT heterostructure.

B. Resistivity and Hall measurements

Figure 3 (a) and (b) show sheet resistance ($R_{\square}$) and Hall resistance (R_{yx}) of pristine BSTS and BSTS/CGT, respectively. The pristine BSTS film exhibited a metallic transport with electron carrier, where $R_{\square}$ monotonically decreased with decreasing T and R_{yx} showed a negative slope linear to the magnetic field (B). Thanks to the highly insulating bulk properties of our BSTS films, contribution of the bulk carriers was suppressed to be negligible, and a surface dominant transport was realized in a wide T, which was able to be decreased further greatly when the film thickness was below 20 nm [26,27,29,30].

After transferring the BSTS film on CGT, the $R_{\square}$ at low Ts below 100 K showed a similar value to that of pristine BSTS, indicating that the transport of TSDS remines dominant in BSTS/CGT heterostructure. Since the carrier density of the CGT substrate increased exponentially by increasing T, the CGT substrate became more conductive than the BSTS film at high Ts. Consequently, the $R_{\square}$ of BSTS/CGT decreased exponentially at above 100 K similarly to that of pristine CGT.

An intriguing drastic change was viewed in R_{yx} of BSTS/CGT as shown in Fig.3 (b). The R_{yx} of BSTS/CGT exhibited a non-linear curvature, corresponding to the multi-channel conduction paths of electrons and high mobility holes arising from TSDSs. The phenomenon can be compared, in strong contrast, to the linear-B dependence observed for pristine BSTS under the same experimental condition. The Hall effect of negative electrons at high B of BSTS/CGT is steeper than that of the pristine BSTS, indicating the reduction in the electron carrier concentration. The carrier concentration of pristine BSTS was estimated to be $n = 6.25 \times 10^{12}$ cm^{-2} by a simple linear curve fitting of the experimental data. For the BSTS/CGT, we carried out a non-linear curve fitting using a parallel circuit model, and estimated the concentration and the mobility of the two carriers as $n = 3.69 \times 10^{10}$ cm^{-2} and $\mu = 3157$ cmV^{-1}s^{-1} for p-type carrier, and $n = 2.44 \times 10^{12}$ cm^{-2} and $\mu = 293$ cmV^{-1}s^{-1} for n-type one. The carrier density of the n-type electrons was comparable to that in the previous works on TI/FMI's, while that of the p-type holes was quite low [12-24], which could be due to the intrinsic nature of low bulk carrier of BSTS and the energy shift of the chemical potential as is discuss below.

Both the suppression of n-type carrier concentration and the appearance in p-type carriers with low carrier density in BSTS/CGT can be explained in terms of the energetically lower shift in chemical potential due to the charge transfer from BSTS to CGT. The TSDS on pristine BSTS and CGT are n-type and p-type material, respectively. Thus, considering a simple P-N junction scheme, the chemical potential of BSTS shifts to lower energy due to the electron transfer from BSTS to CGT as shown in the inset of Fig. 3(b). A similar shift in the chemical potential due to the P-N junction of TI/FMI interface was discussed in the Epi-BST/CGT system [21]. Since the work functions of BSTS and BST are close with each other, the same discussion can be applied to the BSTS/CGT [31]. For the pristine BSTS, the chemical potential of the top surface is considered to be slightly above of that of bottom surface. Furthermore, since the bottom surface is directly connected to CGT, the effect of charge transfer could be stronger at the bottom region than at the top one. Therefore, after contacting the BSTS film to the CGT substrate, the chemical potential of the bottom surface shifted below the Dirac point and showed a low density of p-type carriers, while that of the top surface remained above the DP nevertheless with the reduction in its density.

C. Anomalous Hall Effect in BSTS/CGT heterostructure

One of the most exotic physical phenomena of magnetic-TIs is the AHE, which is expected to be observed when a band gap is generated in TSDS due to the time reversal symmetry break caused by magnetic field. In order to observe the AHE in our BSTS/CGT, an accurate measurement of R_{yx} at low-B region was carried out in a smaller window of T as shown in Fig. 4(a). It is apparent that a positive Hall effect with a greatly steeper gradient was observed within a narrow range in magnetic field of -0.25 T to 0.25 T in addition to the positive slope of hole carrier of TSDS on BSTS. This is considered to be nothing but the AHE as explained later in detail. By subtracting the part showing a linear gradient of hole carriers as the background, the anomalous hall resistance (R_{AH}) can clearly be evident as shown in Fig. 4(b). The R_{AH} has a large positive B dependence and saturates at $B = \pm 0.25$ T with a maximum value reaching R_{AH}=56.3 Ω at 7 K. The magnitude of R_{AH} decreased with an increase in T and disappeared above 100 K.

In order to judge firmly whether the sharp signal observed in R_{yx} at low B originates from the AHE on TSDS, the following two experimental evidences have to be confirmed: (1) whether the observed R_{AH} can be consistent to the B dependence of the magnetization M of CGT, (2) whether T dependence of R_{AH} corresponds to the evolution of magnetization of CGT as a function of T. Figure 5 (a) shows B dependences of $R_{AH}(B)$ for BSTS/CGT and $M(B)$ for CGT at 7 K. The B dependences of these two systems perfectly identically scale with each other, which satisfies the first experimental requirement. Concerning the second point, the R_{AH} of BSTS/CGT was plotted in Fig. 5(b) as a function of T together with the M of CGT. The T dependence of R_{AH} is satisfactorily identical to the $M(T)$ of CGT. Consequently, the R_{yx} experimentally observed for BSTS/CGT fulfills the above two requirements in a satisfactory fashion, being strongly indicative of the fact that we have successful observed the AHE on TSDS in our BSTS/CGT heterostructure via proximity effect. It is noted that the magnitude of AHE to be accessible to the present BSTS/CGT is R_{AH}=56.3 Ω at 7 K, which is 20 times larger than the maximum value in the previous report of BS/YIG, where a similar film-transfer technique was employed [18].

Another concern to be addressed is whether the AHE is originated from the proximity effect at the BSTS/FMI interface or the unintentional doping of Cr atom penetrating into the bottom layer of the BSTS film, which sometime takes place in Epi-TI/FMI systems due to the defects at the TI interface. In our processes, the BSTS film was electrostatically placed on the CGT and chemical interactions at the surfaces are very weak. Furthermore, the annealing temperature of the BSTS/CGT (150℃) is much lower than the melting temperature of each chemical component. In addition, if some amounts of Cr ions are intercalated into the bottom surface of BSTS, they would form a Cr-Bi/Sb layer based on the phase diagram. Actually, the Raman spectra of the BSTS films did not change in each fabrication process, and we can judge that no structural change has occurred in the BSTS films before and after fabricating the BSTS/CGT heterostructure. Finally, in the Cr-doped TI systems, the curie temperature Tc is around 45 K, which is less than that of the ferromagnetic transition of CGT [32]. In our BSTS/CGT, the change of the AH signal matches well to the magnetization evolution of CGT as shown in Fig. 5(a). Considering these reasons, we are plausibly able to conclude that the AHE originates from the proximity effect at the interface.

The magnetic proximity effect in TI/FMI heterostructures is considered to be generated from the influences of the wave functions of TI perturbed by the broken time-reversal symmetry induced by the magnetic field of FMI [33,34]. Since only the bottom topological surface of BSTS contacts with CGT at the interface, the energy gap of the TSDS is considered to be opened in the bottom surface with less influences on the top TSDS.

D. Comparison to the other TI/FMI heterostructures

In order to have a comprehensive understanding of the AHE in TI/FMI heterostructure, it is better to compare not only the value of R_{AH} but also the Anomalous Hall angle, $\tan\theta_{AH} = R_{AH}/R_{xx}$, the latter of which includes the information of both of the R_{AH} and R_{xx} and providing more useful information. Figure 6 summarizes the magnitude of R_{AH} and θ_{AH} at low Ts as a function of carrier density n for various TI/FIM heterostructures so far reported [15-21]. Here, we can classify the data from the aspect of preparation techniques of epitaxial grown TI/FMI (Epi-TI/FMI) [15,17,19-21] and film-transferred TI/FMI (Trs-TI/FMI) [18].

Although many experiments are reported on Epi-TI/FMIs targeting for the proximity magnetic topological heterostructures, merely two reports including our present research are found on Trs-TI/FMI. In our experiments on BSTS/CGT, both of R_{AH} and θ_{AH} were improved; R_{AH} value is 20 times larger and θ_{AH} increases more than one order of magnitude than those of BS/YIG [18].

In the comparison between the present Trs-BSTS/CGT to Epi-TI/FMI's, the Trs-BSTS/CGT shows one-order larger values of R_{AH} and θ_{AH} than those of Epi-TI/FMI's employing YIG, TIG or $LaCoO_3$ substrates [15,17-19]. It should be noticed that, for both Trs- and Epi-TI/FMI's, large values of R_{AH} and θ_{AH} were observed in the heterostructures using CGT as the substrate [20,21]. Since the CGT has the largest magnetization perpendicular to the surface among the FMI substrates shown in Fig.6, it could generate the largest magnetic proximity effect on TI films and lead to large values of R_{AH} and θ_H.

E. The mechanism of magnetic proximity effect in TI/CGT systems

A detail comparison within the heterostructures employing a CGT substrate gives more fundamental discussions about the nature of magnetic proximity effect. The value of θ_{AH} in Trs-BSTS/CGT ($\theta_{AH} = 0.75\%$) is the same as that of BST/CGT given by Yao ($\theta_{AH} = 0.71\%$) [20], while much larger value, ca. 4%, was reported by Mogi et al [21]. Here, the following two important points should be addressed: the quality of the CGT substrate, and the atomic orientation of the TI/CGT interface.

For the first point, while the magnitude of the magnetization of CGT as the substrate is similar among all the three samples, a clear magnetic hysteresis was observed only in the CGT substrate given Mogi et al., which was prepared by the epitaxial growth technique (Epi-CGT). For our BTST/CGT and BST/CGT of Yao et al., the substrate was prepared by the exfoliation technique (Exf-CGT). The disappearance of the hysteresis in the latter case could be due to the smaller magnetic domain size in Exf-CGT than that in the Epi-CGT, which also could lead to a reduction in the magnetic exchange interactions at the TI/CGT interface.

As for the second point, in Epi-TI/FMIs, the constituent atoms of a TI periodically arrange on a FMI so that the lattice mismatching can be reduced as much as possible. Therefore, many locations of magnetic atoms of the FMI would match with those of the constituent atoms of the TI. In Trs-TI/FMI, on the other hand, a TI film will be transferred in a random fashion on a FMI, ending up with the condition that disordered displacement of atoms between the TI and the FMI could be greater. Such disorder has been considered to reduce the exchange interactions between TI and FMI atoms. However, comparing our results on Trs-BSTS/CGT to those of Yao's Epi-BST/CGT, in both of which the same quality CGT substrate is used, the value of θ_{AH} is almost the same. Therefore, it can be concluded that the magnetic proximity effect at the TI/FMI interface has a broad effective field in the in-plane direction, to be compared to the out-of-plane direction [33].

The plausible candidate of such a broad interaction is the magnetic extension [35, 36], which has been considered as one of the microscopic mechanisms of magnetic proximity effect. In this mechanism, the proximity effect is explained by the penetration of the surface state of TI into the FMI. In general, the surface electronic state decays exponentially into the bulk or vacuum, and therefore, the penetration depth is quite small. However, in case of the interface of two materials with a similar crystal structure, the electronic state of TI surface greatly extended into MFI. This phenomenon can be understood as a resonance electronic surface state at the interface of TI/FMI. Since such a surface resonant electronic state is widely effective in the in-plane direction and not sensitive to a small amount of local disordered, it is possible to have a large magnitude of AHE even in the Trs-TI/FNI heterostructure. The relationship between such disorder/order at the interface of TI/FMI and AHE via the magnetic proximity effect is still an important open question in a TI/FM heterostructure system. More accurate studies for various Trs-TI/FMI systems in the future will shed light on the intrinsic nature of AHE and QAHE via the magnetic proximity effect.

4. Conclusions

In conclusion, a large AHE signal was observed in a damage-free BSTS/CGT heterostructure prepared by a wet film transfer method. Both of R_{AH} and θ_H of our Trs-BSTS/CGT showed the highest value among the TI/FMI prepared by the film transfer method thanks to the low carrier density of our high quality BSTS single crystal films. Furthermore, the recorded value of R_{AH} was comparable to the one observed in Van der Waals epitaxial grown TI/FM heterostructures, being indicative of an advantageous point of the film-transfer TI on FMI to be employed as an alternative method via the magnetic proximity effect to achieve AHE/QAHE. The film-transfer technique is simple and can be applicable to a variety of Trs-TIs/FMIs. Experiments are expected to be made in the future by employing better combinations of TIs with higher quality and FMIs with larger magnetization as well as higher Curie temperature.

Acknowledgments

This work was supported in part by a Grant-in-Aid for Scientific Research from the Ministry of Education, Culture, Sports, Science and Technology (MEXT), JSPS KAKENHI Grants (No. 17K14329, 18H04471, 18H04304, 18F18328, and 18H03858) and thermal management of CREST, JST. This work was sponsored by research grants from The Iwatani Naoji Foundation's Research Grant. The research is partly carried out by the support of the World Premier International Research Center Initiative (WPI) from MEXT. K.N thanks for the support of the WISE Program for AI Electronics, Tohoku University.

References

[1] M. Z. Hasan, C. L. Kane, Rev. Mod. Phys. 2010, 82, 3045.

[2] X. L. Qi, T.L. Hughes, S. C. Zhang, Phys. Rev. B 2008, 78, 195424.

[3] R. Yu, W. Zhang, H. J. Zhang, S. C. Zhang, X. Dai, Z. Fang, Science 2010, 329 (5987), 61−64.

[4] C. Z. Chang, J. Zhang, X. Feng, J. Shen, Z. Zhang, M. Guo, K. Li, Y. Ou, P. Wei, L. L. Wang, Z. Q. Ji, Y. Feng, S. Ji, X. Chen, J. Jia, X. Dai, Z. Fang, S. C. Zhang, K. He, Y. Wang, L. Lu, X. C. Ma, Q. K. Xue, Science 2013, 340 (6129), 167−170.

[5] C. Z. Chang, W. Zhao, D. Y. Kim, H. Zhang, B. A. Assaf, D. Heiman, S. C. Zhang, C. Liu, M. H. Chan, J. S. Moodera, Nat. Mater. 2015, 14 (5), 473−477.

[6] Y. Ou, C. Liu, G. Jiang, Y. Feng, D. Zhao, W. Wu, X. X. Wang, W. Li, C. Song, L. L. Wang, W. Wang, W. Wu, Y. Wang, K. He, X. C. Ma, Q. K. Xue, Adv. Mater. 2018, 30 (1), 1703062.

[7] J. G. Checkelsky, R. Yoshimi, A. Tsukazaki, K. S. Takahashi, Y. Kozuka, J. Falson, M. Kawasaki, Y. Tokura, Nat. Phys. 2014, 10 (10), 731−736.

[8] X. Kou, S. T. Guo, Y. Fan, L. Pan, M. Lang, Y. Jiang, Q. Shao, T. Nie, K. Murata, J. Tang, Y. Wang, L. He, T. K. Lee, W. L. Lee, K. L. Wang, Phys. Rev. Lett. 2014, 113 (13), 137201.

[9] W. Wang, Y. Ou, C. Liu, Y. Wang, K. He, Q.-K. Xue, W. Wu, Nat. Phys. 2018, 14 (8), 791−795.

[10] E. O. Lachman, A. F. Young, A. Richardella, J. Cuppens, H. R. Naren, Y. Anahory, A. Y. Meltzer, A. Kandala, S. Kempinger, Y. Myasoedov, M. E. Huber, N. Samarth, E. Zeldov, Sci. Adv. 2015, 1 (10), No. e1500740.

[11] W. Wang, C.-Z. Chang, J. S. Moodera, W. Wu, npj Quantum Materials 2016, 1 (1), 16023.

[12] F. Katmis, V. Lauter, F. S. Nogueira, B. A. Assaf, M. E. Jamer, P. Wei, B. Satpati, J. W. Freeland, I. Eremin, D. Heiman, P. Jarillo-Herrero, J. S. Moodera, Nature 2016, 533 (7604), 513-516.

[13] R. Watanabe, R. Yoshimi, M. Kawamura, M. Moge, A. Tsukazaki, X.Z. Yu, K. Nakajima, K.S. Takahashi, M. Kawasaki, Y. Tokura, Appl. Phys. Lett. 115, 102403 (2019).

[14] P. Chen, Y. Zhang, Q. Yao, F. Tian, L. Li, Z. Qi, X. Liu, L. Liao, C. Song, J. Wang, J. Xia, G. Li, D.M. Burn, G. van der Laan, T. Hesjedal, S. Zhang, X. Kou, Nano Lett. 20, 1731 (2020).

[15] Z. Jiang, C. Z. Chang, C. Tang, P. Wei, J. S. Moodera, J. Shi, Nano Lett. 2015, 15 (9), 5835-5840.

[16] Z. Jiang, C-Z. Chang, C. Tang, J-G. Zheng, J.S. Moodra, J. Shi, AIP Advances 6, 055809 (2016).

[17] C. Tang, C. Z. Chang, G. Zhao, Y. Liu, Z. Jiang, C. X. Liu, M. R. McCartney, D. J. Smith, T. Chen, J. S. Moodera, J. Shi, Sci. Adv. 2017, 3 (6), No. e1700307.

[18] X. Che, K. Murata, L. Pan, Q. L. He, G. Yu, Q. Shao, G. Yin, P. Deng, Y. Fan, B. Ma, X. Liang, B. Zhang, X. Han, L. Bi, Q. H. Yang, H. Zhang, K. L. Wang, ACS Nano 2018, 12 (5), 5042-5050.

[19] S. Zhu, D. Meng, G. Liang, G. Shi, P. Zhao, P. Cheng, Y. Li, X. Zhai, Y. Lu, L. Chen, K. Wu, Nanoscale 2018, 10 (21), 10041-10049.

[20] X. Yao, B. Gao, M-G. Han, D. Jain, J. Moon, J. W. kim, Y. Zhu, S-W. Cheong, S. Oh, Nano Lett. 2019, 19, 4567-4573.

[21] M. Mogi, T. Nakajima, V. Ukleev, A. Tsukazaki, R. Yoshimi, M. Kawamura, K.S. Takahashi, T. Hanashima, K. Kakurai, T.H. Arima, M. Kawasaki, Y. Tokura, *Phys. Rev. Lett.* 123, 016804 (2019).

[22] J.S. Lee, A. Richardella, R.D. Fraleigh, C-X, Liu, W. Zhao, N. Samarth, npj Quant. Mat. 3, 51 (2018).

[23] S.R. Yang, Y.T. Fanchiang, C.C. Chen, C.C. Tseng, Y.C. Liu, M.X. Guo, M. Hong, S.F. Lee, J. Kwo, Phys. Rev. B 100, 045138 (2019).

[24] V.M. Pereira, S.G. Altendorf, C.E. Liu, S.C. Liao, A.C. Komarek, M. Guo, H.-J. Lin, C.T. Chen, M. Hong, J. Kwo, L.H. Tjeng, C.N. Wu, Phys. Rev. Mater. 4, 064202 (2020).

[25] L.D. Alegria, H. Ji, N. Yao, J.J. Clarke, R.J. Cava, J.R. Petta, Appl. Phys. Lett. 105, 053512 (2014).

[26] N. H. Tu, Y. Tanabe, Y. Satake, K. K. Huynh, P. H. Le, S. Y. Matsushita, and K. Tanigaki, *Nano Lett*. 17, 2354 (2017).

[27] N. H. Tu, Y. Tanabe, Y. Satake, K. K. Huynh, and K. Tanigaki, *Nature commun*. **7,** 13763 (2016).

[28] Y. Tian, M.J. Gray, H. Ji, R.J. Cava, K.S. Burch, 2D Materials, 3, 025035 (2016).

[29] S.Y. Matsushita, K. K. Huynh, H. Yoshino, N. H. Tu, Y. Tanabe, and K. Tanigaki, Phys. Rev. Mater. 1, 054202 (2017).

[30] S.Y. Matsushita, K.K. Huynh, K. Tanigaki, Phys. Rev. B 99, 195302 (2019).

[31] D. Takane, S. Souma, T. Sato, T. Takahashi, K. Segawa, Y. Ando, Appl. Phys. Lett. 109, 091601 (2016).

[32] J.G. Checkelsky, R. Yoshimi, A. Tsukazaki, K.S. Takahashi, Y. Kozuka, J. Falson, M. Kawasaki, Y. Tokura, Nat. Phys., 10, 731 (2014).

[33] W. Luo, X.-L. Qi, Phys. Rev. B 2013, 87 (8), 085431.

[34] S. V. Eremeev, V. N. Men'shov, V. V. Tugushev, P. M. Echenique, E. V. Chulkov, Phys. Rev. B 2013, 88 (14), 144430.

[35] M. M. Otrokov, T.V. Menshcuikova, M.G. Vergniory, I. P. Rusinov, A. Yu Vyazooskaya, Yu. M. Koroteev, G. Bihlmayer, A. Ernst, P. M. Echenique, A. Arnau, E. V. Chulkov, 2D Mater. 4, 025082 (2017)

[36] S. Bhattacharya, G. Akhgar, M. Gebert, J. Karel, M. T. Edmonds, M. S. Fuhrer, arXiv:2012.11248v1 (2020).

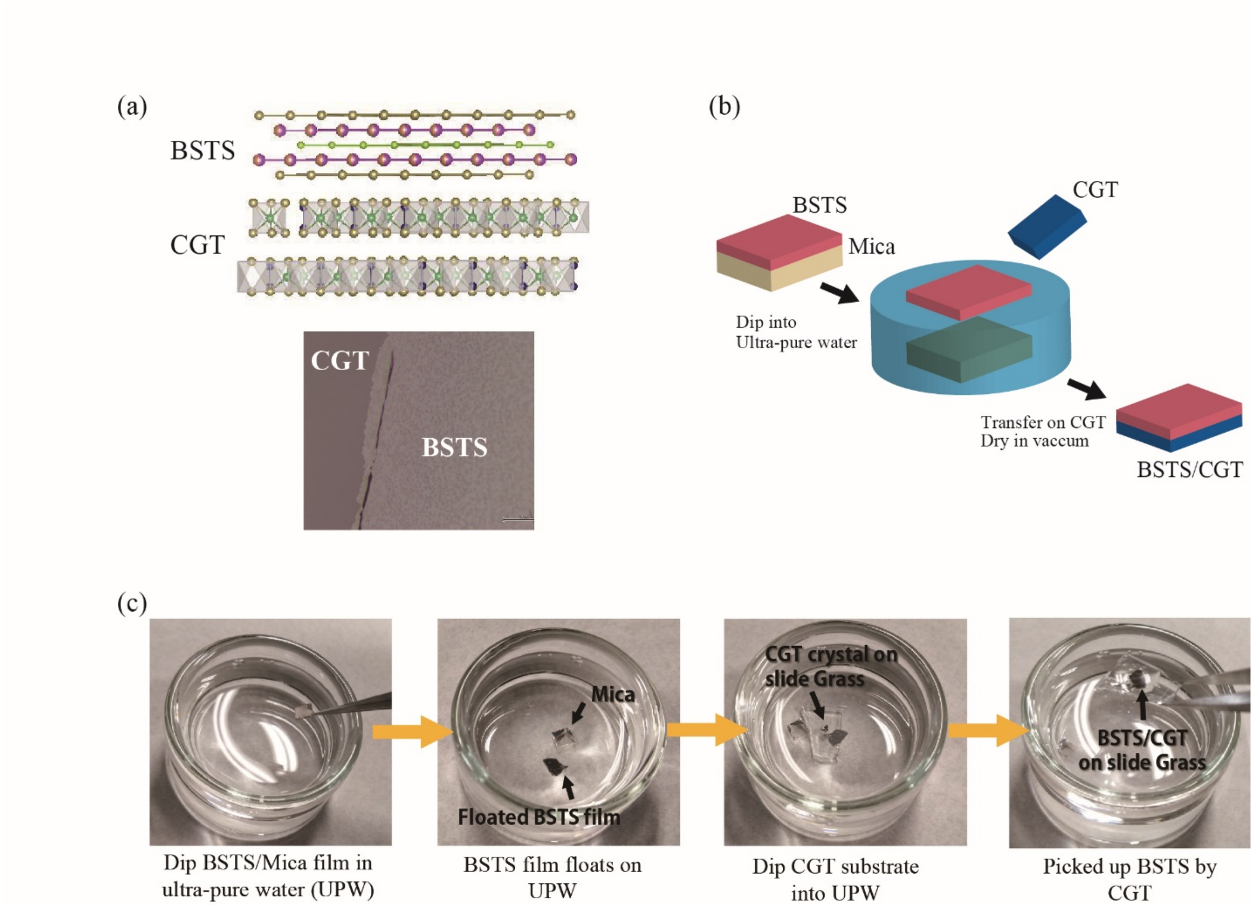

Figure 1. Schematic model of BSTS/CGT heterostructure and its preparation processes. (a) Schematic model of BSTS/CGT structure and optical image in 200×200 μm². (b) Schematic model of Film-transferred BSTS/CGT preparation processes. (c) The detail processes for each preparation step.

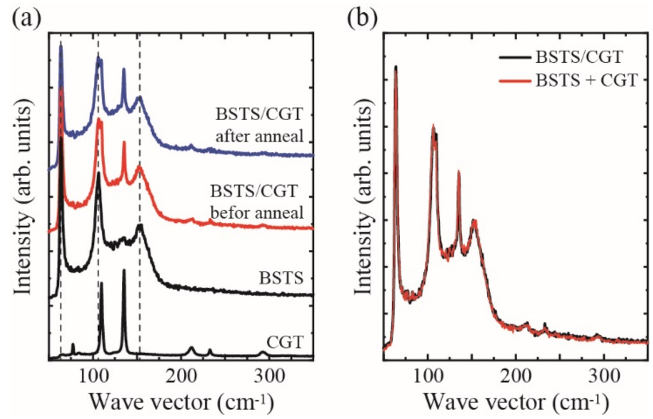

Figure 2. Raman spectra of pristine BSTS, CGT and BSTS/CGT heterostructure. (a) The Raman spectra of the samples corresponding to each preparation process. (b) Comparison between the Raman spectra of BSTS/CGT heterostructure (black) and the sum of the pristine BSTS and CGT (red). The spectra in red were calculated by a linear combination of both BSTS and CGT spectra in (a) as $I_{tot}=I_{BSTS} + 0.6*I_{CGT}$.

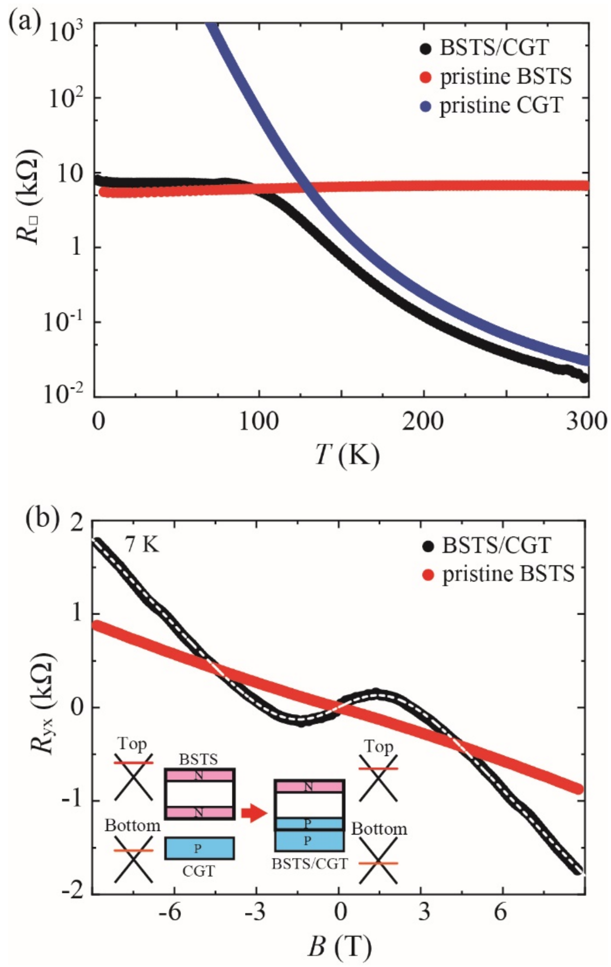

Figure 3. The electronic transport of BSTS/CGT heterostructure. (a) Sheet resistance of BSTS/CGT, pristine BSTS film and CGT flake. The thickness of the BSTS film is 21 nm, which is thin enough to suppress the bulk contributions to realize the surface dominant transport. (b) Hall resistivity of BSTS/CGT and pristine BSTS film at 7 K. The fitting curve of the Hall resistivity of BSTS/CGT base on the parallel circuit model is shown as a white dashed line. The inset in (b) is a schematic image of the band picture of before and after transferring BSTS on CGT. Due to the p-n junction formed at the interface of CGT and the bottom surface of BSTS, the chemical potential of BSTS shifts to the lower energy level by ending up the bottom BSTS changes from n- to p-type.

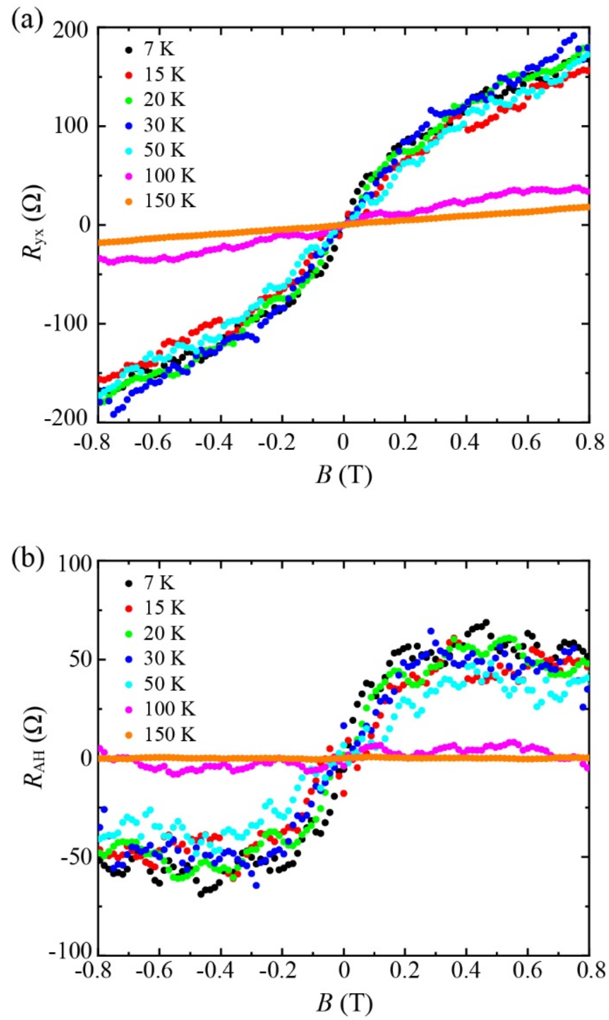

Figure 4. AHE in BSTS/CGT heterostructure. (a) Hall resistivity at low-B (b) R_{AH} under low-B. The R_{AH} was extracted by subtracting the positive slope contributed by hole carriers as the background.

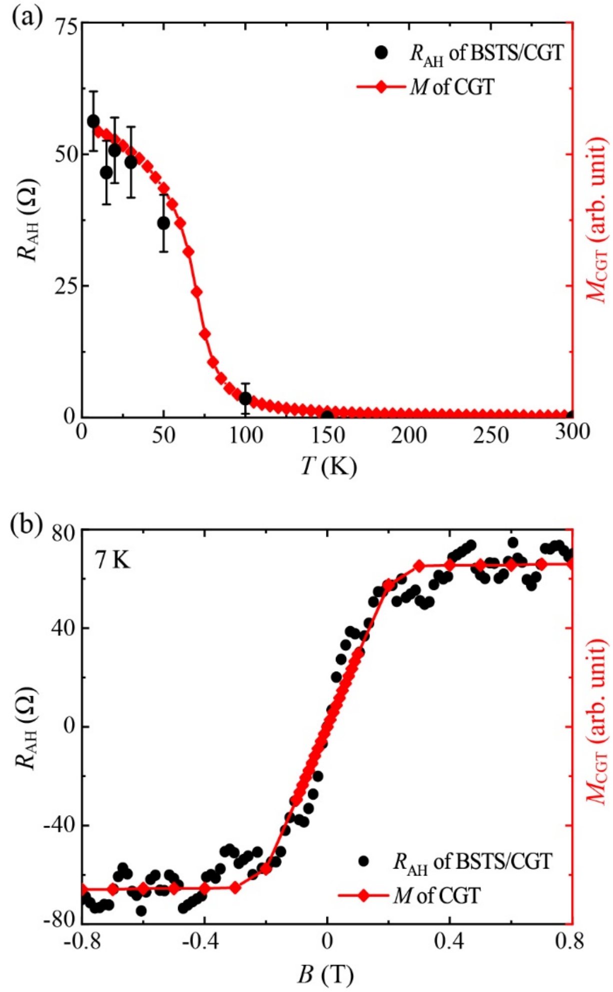

Figure 5. Comparison between R_{AH} of BSTS/CGT and that of the pristine CGT at 7 K. (a) Temperature dependence of R_{AH} of BSTS/CGT and magnetization of CGT substrate. (b) B dependence of R_{AH} of BSTS/CGT and magnetization of CGT. In the figures, the whole behaviors between $R_{AH}(T,B)$ and $M(T,B)$ are perfectly match with each other, which are the firm evidence to confirm the successful observation of AHE in BSTS/CGT.

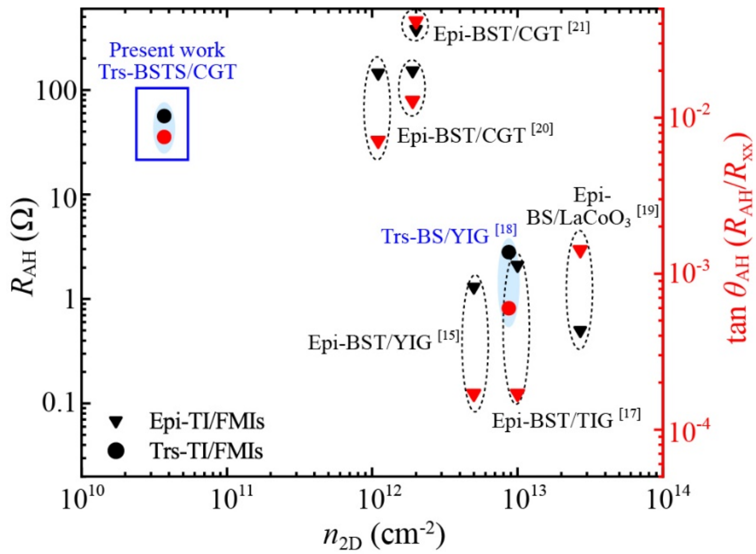

Figure 6. Summary of R_{AH} and θ_{AH} among proximity-induced TI/FMI systems at around 2-7 K. The values of R_{AH} and θ_{AH} of Epi-growth systems (triangles) and film-transferred systems (circles). These data are taken from Ref [15,17-21] are plotted as a function of carrier density together with the present work.